

## Synthesis of Nano- and Micro-Particles of $\text{LiMn}_2\text{O}_4$ : Electrochemical Investigation and Assessment as a Cathode in Li Battery

M.A. Kiani<sup>1</sup>, M.F. Mousavi<sup>1,\*</sup>, M.S. Rahmanifar<sup>2</sup>

<sup>1</sup> Department of Chemistry, Tarbiat Modares University, P.O. Box 14115-175, Tehran, Iran

<sup>2</sup> Faculty of basic science, Shahed University, Tehran, Iran

\*E-mail: [mfmousavi@yahoo.com](mailto:mfmousavi@yahoo.com)

Received: 9 March 2011 / Accepted: 30 May 2011 / Published: 1 July 2011

---

Micro- and nano-particles of  $\text{LiMn}_2\text{O}_4$  are synthesized from micro- and nano-particles of  $\text{MnO}_2$ , respectively. Synthesis of  $\text{MnO}_2$  in the presence of stirrer leads to micro-particles, however, in the presence of ultrasonic waves nano-particles obtained. Both micro- and nano-particles prepared are converted to  $\text{LiMn}_2\text{O}_4$ . The products are characterized by X-ray diffraction (XRD), Scanning Electron Microscopy (SEM) and measurement of surface area (BET). The electrochemical properties of these materials as a cathode in a lithium battery are examined by using the cyclic voltammetry (CV), electrochemical impedance spectroscopy (EIS) and galvanostatic charge/discharge tests. The obtained voltammograms show a pair of oxidation peaks and a pair of reduction peaks with better reversibility for nano-particles. Nyquist plots show lower charge transfer resistance for nano-particles compared with micro-one. Battery charge and discharge test is carried out at different constant currents. It is found that the  $\text{LiMn}_2\text{O}_4$  micro- and nano-particles deliver 85 and 146  $\text{mAh g}^{-1}$  (3.0–4.5 V) in the first cycle and 62 and 141  $\text{mAh g}^{-1}$  discharge capacity after 50 cycles, respectively. The micro-particles suffer from capacity fading but the nano-particles show much improved capacity retention (24%).  $\text{LiMn}_2\text{O}_4$  nano-particles exhibit the better rate of performance in comparison with the micro-one.

---

**Keywords:**  $\text{LiMn}_2\text{O}_4$ , nano-particles, sonochemical method, lithium battery

### 1. INTRODUCTION

Nanomaterials have been widely used in life sciences, information technology, environment, and especially attracted attention for application in energy storage devices [1, 2], particularly for those with high charge/discharge current rates such as lithium batteries [3, 4]. Lithium rechargeable batteries have numerous challenges for development especially on cathodic materials [5]. Transition metal

oxides, due to their high electrochemical potentials, high reversible lithium insertion/deinsertion and high capacity for lithium storage are much more interest as a cathode materials for Li batteries [6]. There is a multitude of literature available on the synthesis, structural, and electrochemical studies of metal oxides such as Co, Mn, Ni, Mo and V with regard to lithium battery cathodes [7]. Among numerous transition-metal oxides, manganese oxide based compounds are particularly attractive as cathodes because of their low cost, abundance, and nontoxicity [8, 9]. Among them, spinel  $\text{LiMn}_2\text{O}_4$  has emerged as one of the promising candidates because of its three-dimensional  $\text{Li}^+$  diffusion and high theoretical capacity of  $148 \text{ mAh g}^{-1}$  [10]. Nonetheless, the spinel  $\text{LiMn}_2\text{O}_4$  suffers from capacity fading during cycling, which has been a key problem prohibiting  $\text{LiMn}_2\text{O}_4$  from commercialization. Thus, great efforts have been done for obviation of this defect.

The electrochemical properties of the electrode materials strongly depend on the physical and chemical properties such as particle size, morphology, stoichiometry and homogeneity [11, 12]. Particle size seems to be a criterion affecting the electrochemical performance of cathode materials in Li batteries. To use nanomaterials is one of the effective ways to improve performances of Li batteries [13-15]. Although diffusion of Li-ion is not really fast through active materials, the diffusion paths can be shortened by use of small-size powders of active materials. It seems that the next generations of rechargeable power sources may use extensively electrodes prepared from nano-sized particles.

Several techniques such as hydrothermal [16], sol-gel [17], combustion [18, 19], precipitation [20], emulsion drying [21], spray pyrolysis [22] and mechanochemical methods [23, 24] have been adopted for the synthesis of nano-crystalline materials which they use in Li batteries as a cathode material.

Sonochemical synthesis is an effective method for the chemical synthesis of nano-structured materials with well controlled shape, size, and structure [25-31]. During sonication process, ultrasonic sound waves radiate through the solution causing alternating high and low pressures in the liquid medium. Millions of microscopic bubbles form and grow in the low pressure step and collapse in the high pressure step [32]. The implosive collapse of the bubbles generates localized hot spots through adiabatic compression or shock wave formation within the gas phase of the collapsing bubble. These hot spots have been shown to have transient temperatures of about 5000-25000 K, pressure of 1800 atm, and cooling rates in excess of  $10^{11} \text{ K s}^{-1}$  [33]. More details about the growth of the nuclei, the kinetics and application of ultrasound to the synthesis of a wide range of materials have also been reported in related papers [34, 35].

Some comparative studies between micro- and nano-materials performances as active material in Li batteries have been done by researchers. Kovacheva et al. reported a comparative analysis of the electrochemical characteristics of thin-layer  $\text{LiNi}_{0.5}\text{Mn}_{1.5}\text{O}_4$  intercalation electrodes comprised of micro- or nano-sized particles [36].

Chen and coworkers prepared nano- and micro-sized  $\text{LiNi}_{0.5}\text{Mn}_{1.5}\text{O}_4$  particles via the thermal decomposition of a ternary eutectic Li-Ni-Mn acetate and investigated electrochemical properties of them [37]. Shaju et al. synthesized nano- $\text{LiMn}_2\text{O}_4$  by a one-pot resorcinol-formaldehyde route and compared nano-structured  $\text{LiMn}_2\text{O}_4$  with sol-gel method obtained  $\text{LiMn}_2\text{O}_4$  [14]. Results of these studies suggest that nano-particles exhibit excellent rate capability, retaining its capacity at high rates and nano-particles may possess a stabilized surface that inhibits dissolution. In another work,

Kamarulzaman et al. prepared  $\text{LiMn}_2\text{O}_4$  nano- and normal-powders using the high-energy ball milling and sol-gel methods, respectively [15]. They offered that lowering of the surface energy of the nanomaterials occurs and explains the improved performance and the decrease in capacity fade.

Following our previous work on our comparative study between micro- and nano-particles of  $\beta\text{-Ni(OH)}_2$  [38] as nickel battery cathode material and other works on electrochemical energy storage systems, such as polyaniline battery [39-46], lead-acid battery [47, 48] and supercapacitor [49], in this work, we have developed and demonstrated a two-step method for the utilization of commercially cheap nano-particles of  $\text{LiMn}_2\text{O}_4$  spinel as a cathode material for Li-ion batteries. In previous works, we also adopted a sonochemical method for synthesis of nano-materials such as  $\beta\text{-PbO}_2$  [50] and  $\beta\text{-Ni(OH)}_2$  [38].

In the present study, we first synthesized  $\gamma\text{-MnO}_2$  nano-particles by sonochemical method, and used as precursor for synthesis of  $\text{LiMn}_2\text{O}_4$  nano-particles. To reduce the particle size of  $\text{LiMn}_2\text{O}_4$  final products, the particle size of the  $\text{MnO}_2$  was controlled via ultrasonic irradiation. A comparative study between nano-particles synthesized by this method and micro-particles as a cathode material in Li battery has been done.

## 2. EXPERIMENTAL

### 2.1. Apparatus

A multiwave ultrasonic generator (Sonicator® 3000; Misonix, Inc., Farmingdale, NY, USA), equipped with a converter/transducer and titanium oscillator (horn), 12.5mm in diameter, operating at 20 kHz with a maximum power output of 600 W, was used for the ultrasonic irradiation. The ultrasonic generator automatically adjusted the power level. The wave amplitude in each experiment was adjusted as needed.

A cylindrical two-walled glass cell with an interior volume of 300 mL was used for the sonication of the reaction solution. The solution temperature was kept constant by circulating water from a water bath (Optima, Tokyo, Japan). A home-made centrifuge, with a maximum speed of 8000 rpm, was used for the deposition of dispersed nano-particles. For milling precursors, we used Retsch mixer/mill (RM 100) instrument. An electrical furnace (Paragon E10, USA) was used to heat the samples. The CV and EIS measurements were carried out using Galvanostat/Potentiostat Autolab (PGSTAT30) connected to a PC. Electrochemical charge/discharge was measured with a Solartron SI 1470.

### 2.2. Synthesis of nano- and micro- $\text{LiMn}_2\text{O}_4$ particles

First, micro- and nano-particles of  $\text{MnO}_2$  were prepared. Briefly, micro and nano-particles of  $\gamma\text{-MnO}_2$  were synthesized by redox reaction between stoichiometric quantities of  $\text{MnSO}_4\cdot\text{H}_2\text{O}$  and  $(\text{NH}_4)_2\text{S}_2\text{O}_8$  (Merck) in aqueous medium. The redox reaction between manganese sulphate and ammonium peroxydisulphate was adopted for synthesis of  $\gamma\text{-MnO}_2$ . For this purpose, 100 mL of

MnSO<sub>4</sub>·H<sub>2</sub>O and 100 mL of (NH<sub>4</sub>)<sub>2</sub>S<sub>2</sub>O<sub>8</sub> solutions with definite concentrations were mixed together in reaction vessel. Synthesis of micro-particles was carried out in the presence of stirrer and synthesis of nano-particles was done in the presence of ultrasonic wave and the solution was sonicated for 1 h. Then the solution was centrifuged at 7500 rpm for 5 min.

A dark brown precipitate was obtained, washed several times with double distilled water and dried in an oven at 80 °C for 6 h. Micro-particles of  $\gamma$ -MnO<sub>2</sub> were synthesized in the absence of ultrasonic irradiation. Synthesis of nano-LiMn<sub>2</sub>O<sub>4</sub> (or micro) was carried out by mixing stoichiometric amounts of nano-MnO<sub>2</sub> (or micro) and LiOH (Merck), (2:1 in mol ratio) and milling for 1 h. Mixed precursors were heated at various temperatures (400-900 °C) for 6 h. The resulting powders were thoroughly washed with distilled water and ethanol to remove residual lithium salt and then dried at 110 °C.

### 2.3. Characterization and Electrochemical investigation

X-ray diffraction (Cu K $\alpha$ ,  $\lambda = 1.5406 \text{ \AA}$ ) (Philips X'pert diffractometer), scanning electron microscopy (SEM) (Philips XL 30) were used to characterize the as-prepared powders. Surface area measurements were obtained using the Brunauer, Emmett, and Teller (BET) method employing a BEL Japan, Inc. instrument and nitrogen gas.

The electrochemical performance of the as-prepared powders was investigated with a beaker-type three-electrode cell. The working electrode was composed of 80% LiMn<sub>2</sub>O<sub>4</sub>, 15% carbon (Merck) and 5% Teflon (polytetrafluoroethylene) (60 % water based solution from SUTECH, Iran) binder by weight. And then, the blend was rolled and pressed onto a nickel grid current collector, and the electrode was dried at 120 °C for 12 h in oven. The weight of active materials for fabricating electrode in each experiment was exactly equal. The three-electrode cell consisted of a working electrode and a pressed Li granule (Fluka) on a Ni grid current collector was used for the electrochemical measurement as counter and reference electrode. The electrolyte was 1M LiClO<sub>4</sub> (Acros) in propylene carbonate (PC) (Merck).

The assembly of the cells was carried out in a dry Ar-filled glove box. Cyclic voltammogram was measured at a sweep rate of 0.1 mVs<sup>-1</sup> between 3.2 and 4.5 V. The EIS experiments were performed at different applied voltages (3.7-4.4 V) over a frequency range of 100 kHz to 10 mHz with a perturbation amplitude of 5 mV, using an ac signal, with at least 7 points per decade which were logarithmically spaced.

Data analysis was done based on CNLS method of Boukamp using Zview2 software (Scribner Associates), using an appropriate equivalent circuit described in the text. It should be noted that in all cases, the uncertainty in data fitting was approximately less than 10%. The CV and EIS measurements were carried out using Galvanostat/Potentiostat Autolab (PGSTAT30) connected to a personal computer.

The electrochemical cell for charge/discharge studies was composed of a composite cathode, 1M LiClO<sub>4</sub> in PC as electrolyte, and lithium metal as the anode. Galvanostatic charge/discharge

measurements were performed within a potential range of 3.0–4.5V versus Li/Li<sup>+</sup>. The electrochemical tests were applied at 25 °C under argon atmosphere.

### 3. RESULTS AND DISCUSSION

#### 3.1. XRD studies

Good crystallinity is the critical parameter in determining the electrochemical performance of cathode materials. Heat treatment effect on the structure of prepared oxides was investigated at wide temperature range (400–700 °C). The XRD patterns of the samples are shown in Fig. 1.

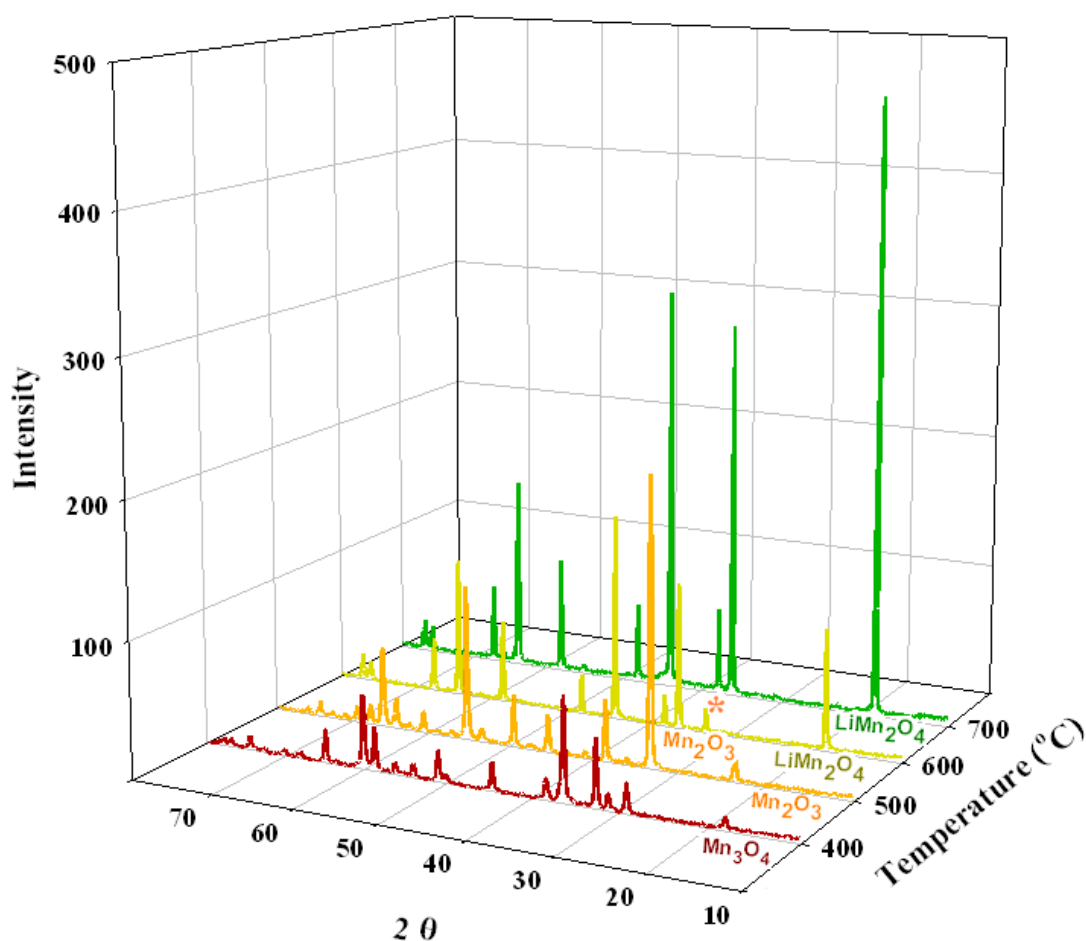
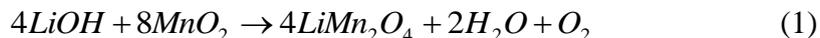


**Figure 1.** XRD patterns of heat treatment prepared oxides.

As can be seen in this figure, Mn<sub>3</sub>O<sub>4</sub> at 400 °C and Mn<sub>2</sub>O<sub>3</sub> at 500 °C are the only products, but at 600 °C, a mixture of LiMn<sub>2</sub>O<sub>4</sub> and Mn<sub>2</sub>O<sub>3</sub> as impurity was observed. Further, with an increase in temperature up to 700 °C, the XRD pattern showed pure LiMn<sub>2</sub>O<sub>4</sub>. The XRD pattern of the sample heated at 700 °C substantiates the formation of highly crystalline proposed product (LiMn<sub>2</sub>O<sub>4</sub>). All the

diffraction peaks in the experimental pattern can be indexed to an octahedral phase of  $\text{LiMn}_2\text{O}_4$ . No peaks from other phases have been detected, indicating the high purity of the product. The  $\text{LiMn}_2\text{O}_4$  XRD diffractogram showed features of the spinel structure with  $Fd3m$  space group (JCPDS card No. 350782). A possible chemical reaction in the synthesis of  $\text{LiMn}_2\text{O}_4$  might be as follows:



According to this reaction,  $\text{Mn}^{4+}$  ions were reduced by  $\text{OH}^-$ , leading to mixed valences of  $\text{Mn}^{4+}/\text{Mn}^{3+}$  in the reaction system. Oxygen was released as the result of oxidation of  $\text{OH}^-$  by  $\text{Mn}^{4+}$ . Also at higher temperatures (800 and 900 °C), impurity of  $\text{Mn}_2\text{O}_3$  was observed again (data not shown), which is related to evaporation of lithium salts and deficiency of lithium in mol ratio.

### 3.2. SEM and BET studies

The SEM micrographs of the micro- and nano- samples are given in Fig. 2a and b, respectively.

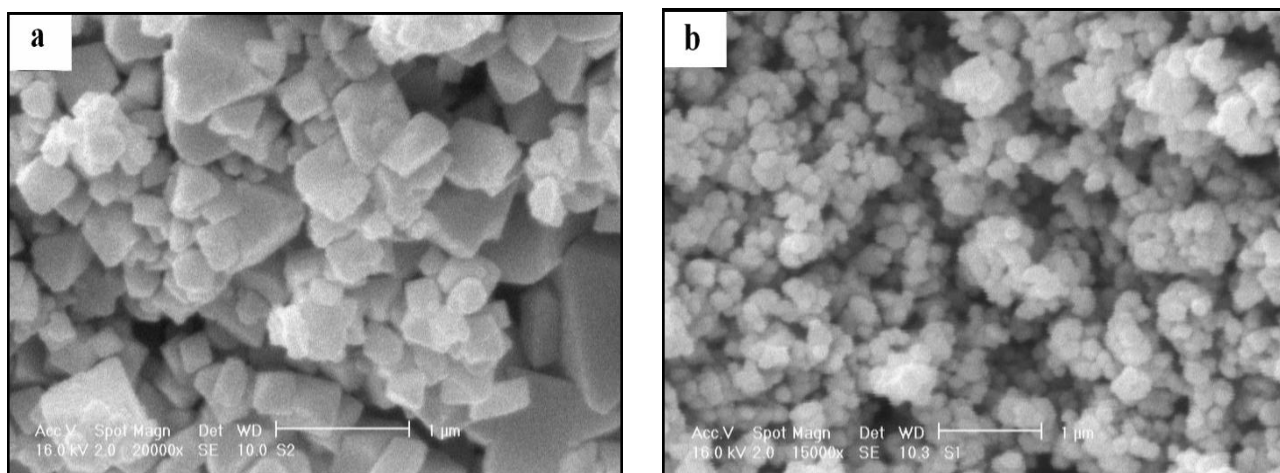


**Figure 2.** SEM micrograph of  $\text{LiMn}_2\text{O}_4$  (a) micro-particles and (b) nano-particles.

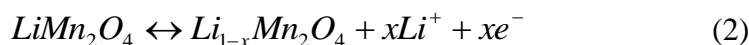
As seen in Fig. 2a, the as-prepared micro-particles show a cubic-like morphology with different dimensions. The micrograph of nano-particles shows an almost uniform spherical morphology (Fig. 2b). The nano-particles have a rough surface and smaller size, while the micro-particles have a larger taping particle and very smooth surface. The average sizes of the samples were about 290 and 35 nm for micro- and nano-particles, respectively.

$\text{N}_2$  adsorption-desorption studies were performed to determine the specific surface area of the  $\text{LiMn}_2\text{O}_4$  micro- and nano-particles. The BET surface area was found to be 6.8 and  $74.6 \text{ m}^2\text{g}^{-1}$  for micro- and nano-particles respectively, which shows about 11 times increase in surface area.

### 3.3. Electrochemical studies

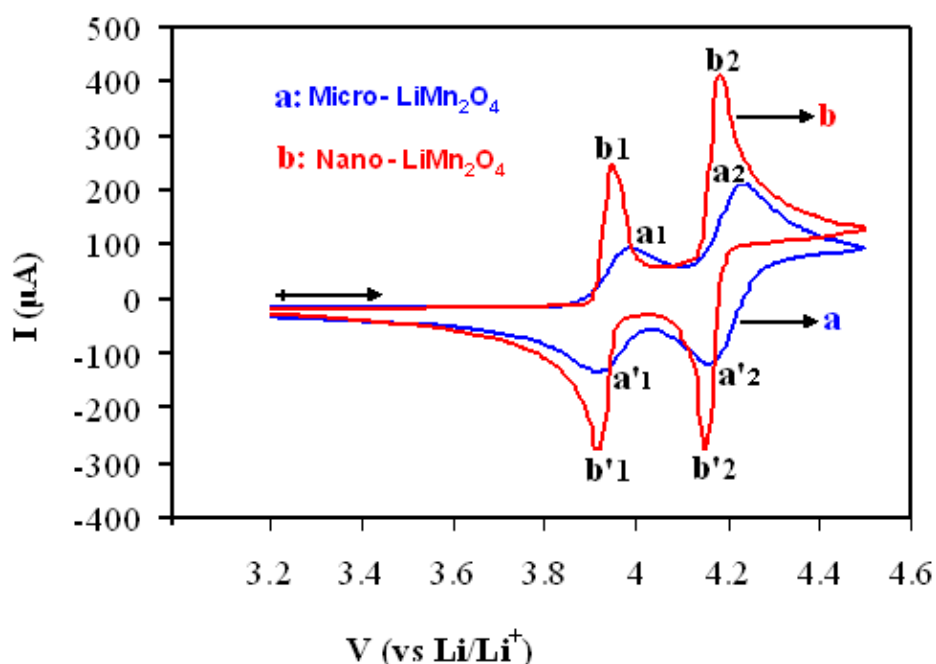
#### 3.3.1. CV

Fig. 3a and b shows cyclic voltammograms of  $\text{LiMn}_2\text{O}_4$  micro- and nano-particles, respectively in scan rate of  $0.1 \text{ mV s}^{-1}$ . Two pairs of redox peaks were observed for micro- and nano-particles owing to the insertion /deinsertion of lithium ion at  $\text{LiMn}_2\text{O}_4$ :



Equation 2 is a typical characteristic attributed to the (de)intercalation process of Li ion in 8a tetrahedral sites of  $\text{LiMn}_2\text{O}_4$  spinel [15]. The first peak is attributed to the removal of lithium ions from the tetrahedral sites where Li–Li interactions occur, whereas the second peak is attributed to the removal of lithium ions again from the tetrahedral sites but where Li–Li interaction does not occur. Nano-particles show more than 2.5 times higher peak current than micro-particles in all corresponding peaks.

The peaks for the  $\text{LiMn}_2\text{O}_4$  nano-particles are sharper than  $\text{LiMn}_2\text{O}_4$  micro-particles. The narrower peak in the CV curve implies that a specific electrochemical reaction completes at a shorter period of time. In the present case, the narrower peak indicates that the (de)intercalation process of Li ion can take place at a more rapid rate. Some peak parameters for micro- and nano-particles are listed in Table 1.



**Figure 3.** Cyclic voltammograms of  $\text{LiMn}_2\text{O}_4$  (a) micro-particles and (b) nano-particles electrode at scan rate of  $0.1 \text{ mV s}^{-1}$  using  $1 \text{ M LiClO}_4$  as electrolyte in PC at  $25 \text{ }^\circ\text{C}$ .

**Table 1.** Electrochemical parameters from CV for micro- and nano-particles of  $\text{LiMn}_2\text{O}_4$ .

Parameter	$E_{p1}$ (V)	$E_{p2}$ (V)	$E'_{p1}$ (V)	$E'_{p2}$ (V)	$\Delta E_{p1}$ (mV)	$\Delta E_{p2}$ (mV)	$\frac{I_{Pa1}}{I_{Pc1}}$	$\frac{I_{Pa2}}{I_{Pc2}}$
(a) Micro-	3.991	4.240	3.911	4.160	80	80	1.33	0.86
(b) Nano-	3.952	4.181	3.922	4.151	30	30	1.05	0.96

The peak separations ( $\Delta E_p$ ) for micro- and nano-particles are 80 and 30 mV, respectively. The less peak separation and equal peak currents of nano-particles indicate that they have more reversible behavior than micro-particles. With decreasing particle size, an increasing proportion of the total number of atoms lies near or on the surface, making the electrochemical reactivity of the particles more and more important. Both CVs (micro and nano) have a larger  $\Delta E_p$  than ideal condition ( $\Delta E_p=0$ ), which means that  $\text{Mn(III)} \leftrightarrow \text{Mn(IV)}$  reaction is controlled by insertion/deinsertion of  $\text{Li}^+$  in cathodic materials. Shorter lithium ion path causes faster reaction, where smaller  $\Delta E_p$  has been obtained. This condition is substantiated by using nano-particles and  $\Delta E_p$  has been reduced from 80 to 30 mV. The peak broadening for micro-particles is greater than nano-particles. The use of large particles or thick films of active materials, which have long diffusion paths of lithium-ion, gives diffusional behavior of lithium-ion through the active materials, therefore, broad redox peaks due to the insertion and extraction of lithium ion should be observed in cyclic voltammograms [51]. In this work, electroactive nano-particles were pressed on a nickel substrate. Hence, the influence of the diffusional behavior of lithium-ion through the  $\text{LiMn}_2\text{O}_4$  nano-particles was apparently suppressed, and sharp redox peaks were observed in the cyclic voltammogram. In addition, comparison of peak current ratios for micro- and nano-particles shows that the charge on oxidation process is the same as that reduction step for nano-particles, but on micro-particles, this parameter is deviate from unit. On the other hand, the current ratios show that exchange charge on redox process is equal in nano-particles but in micro-particles is not equal.

### 3.3.2. EIS

Fig. 4 displays the typical Nyquist ac impedance results for the test cells composed of the  $\text{LiMn}_2\text{O}_4$  cathodes as the function of the dc bias cited potentials versus a  $\text{Li/Li}^+$  electrode.

In general, the impedance curves present two partially overlapped semi-circles in the high and medium frequency regions and an inclined line in the low frequency region. The first semi-circle at higher frequency is correlated with the formation of a passivation film on the surface and the second semi-circle at lower frequency is related to the  $\text{Li}^+$  charge transfer at the interface [52], while the linear portion is designated to Warburg impedance ( $W$ ), which is attributed to the diffusion of lithium ions into the bulk of the electrode materials.

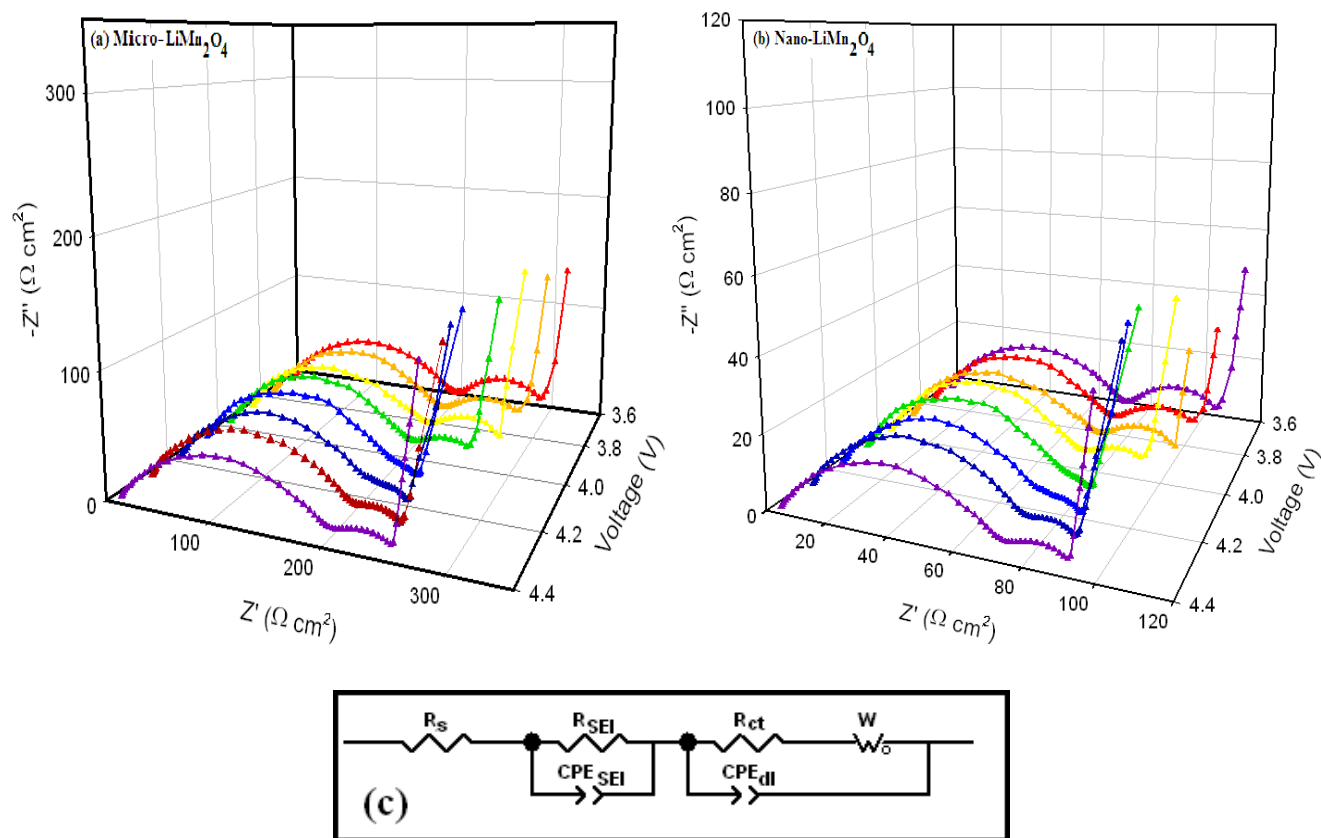


**Figure 4.** Potential effect on nyquist plots of  $\text{LiMn}_2\text{O}_4$  (a) micro-particles and (b) nano-particles electrodes at different applied voltages (vs  $\text{Li}/\text{Li}^+$ ) from 100 kHz to 10 mHz, (c) equivalent circuit.

The resistance of solution ( $R_s$ ) and the resistance of solid electrolyte interface ( $R_{SEI}$ ) changed just a little because the electrolyte and the surface film were stable during cycling for the cell and they are potential-independent. The test cell impedance mainly attributed to charge-transfer resistance of cathode. As indicated in the Fig. 4, the diameter of the first semi-circle has no obvious change, by contrast, a pronounced difference appears at the diameter of the second semi-circle, which mainly reflects the change of charge-transfer resistance. The increase of charge-transfer resistance would bring the capacity fading during the cycling [53]. An equivalent circuit used to fit the impedance data is given in Fig. 4, which is similar to the circuit employed for the cathode of the lithium ion battery. The calculated parameters of impedance spectra in Fig. 4 based on equivalent circuit are listed in Table 2.

**Table 2.**  $R_{ct}$  ( $\Omega \cdot \text{cm}^2$ ) fitted values from EIS for micro- and nano-particles of  $\text{LiMn}_2\text{O}_4$  at different applied voltages.

Voltage (V)	3.70	3.80	3.90	4.00	4.10	4.20	4.30	4.40
(a) Micro-	95	85	82	70	28	40	45	64
(b) Nano-	39	35	31	25	10	15	18	22

The results show that the charge transfer resistance decreased for both micro- and nano-particles with increasing the electrode potential from 3.7 to 4.1V, and then increased with increasing the potential from 4.2 to 4.4V, however micro-particles show about 3 times higher charge transfer resistance and this proportion remain approximately constant at entire examined potentials. This behavior shows good consistency with CV-grams. This tendency is typical for the  $\text{LiMn}_2\text{O}_4$  as reported by other groups [52, 54]. Reducing charge transfer resistance causes discharging the battery with the higher current value.

### 3.3.3. Charge/Discharge test

Electrodes, which were fabricated with both micro- and nano-particles of  $\text{LiMn}_2\text{O}_4$ , were subjected to electrochemical charge/discharge in 1.0 M  $\text{LiClO}_4$  electrolyte in PC. A typical charge/discharge curve at a rate of  $C/2$  ( $C = 148 \text{ mA g}^{-1}$ ), in the potential window of 3.0-4.5 V, for micro- and nano-particles are shown in Fig.5.

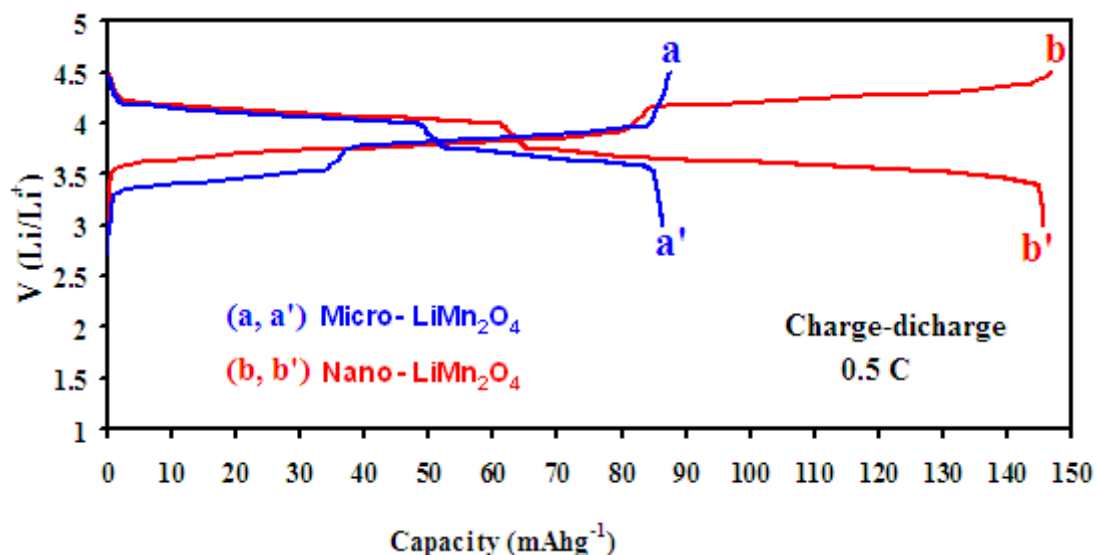


**Figure 5.** Charge/discharge curves of  $\text{LiMn}_2\text{O}_4$  tested at rate of 0.5 C between 3.0 and 4.5 V. (a, a') micro-particles (b, b') nano-particles.

The charge/discharge curves of the  $\text{LiMn}_2\text{O}_4$  micro- and nano-particles both presented two plateaus corresponding to CV diagrams. Both charge and discharge curves of nano-particles have higher specific capacity than micro-particles. As can be seen from this figure, discharge capacity for micro- and nano-particles is 85 and 145  $\text{mAhg}^{-1}$ , respectively. The promotion in the specific capacity shown by the nano-particles can be explained by their small particle size, due to their high surface area to volume ratio. The reversibility of the electrochemical process is also observed in charge/discharge curves. The increase in the surface area to volume ratio enhances the efficiency of the electrochemical intercalation and de-intercalation of the  $\text{Li}^+$  ions in and out of the host material. The transportation of the  $\text{Li}^+$  ions is facilitated when the ratio of atoms on the surface to those in the interior is larger. The

improved specific capacity can also be attributed to the shorter path length that has to be passed by the  $\text{Li}^+$  ions within the nano-materials. This expedites the transportation of ions through the cathode material into the electrolyte and on to the anode that is necessary in a Li rechargeable battery at high rate.

To clarify the kinetic behavior of lithium-ion transfer, the discharge tests were carried out at different rates.

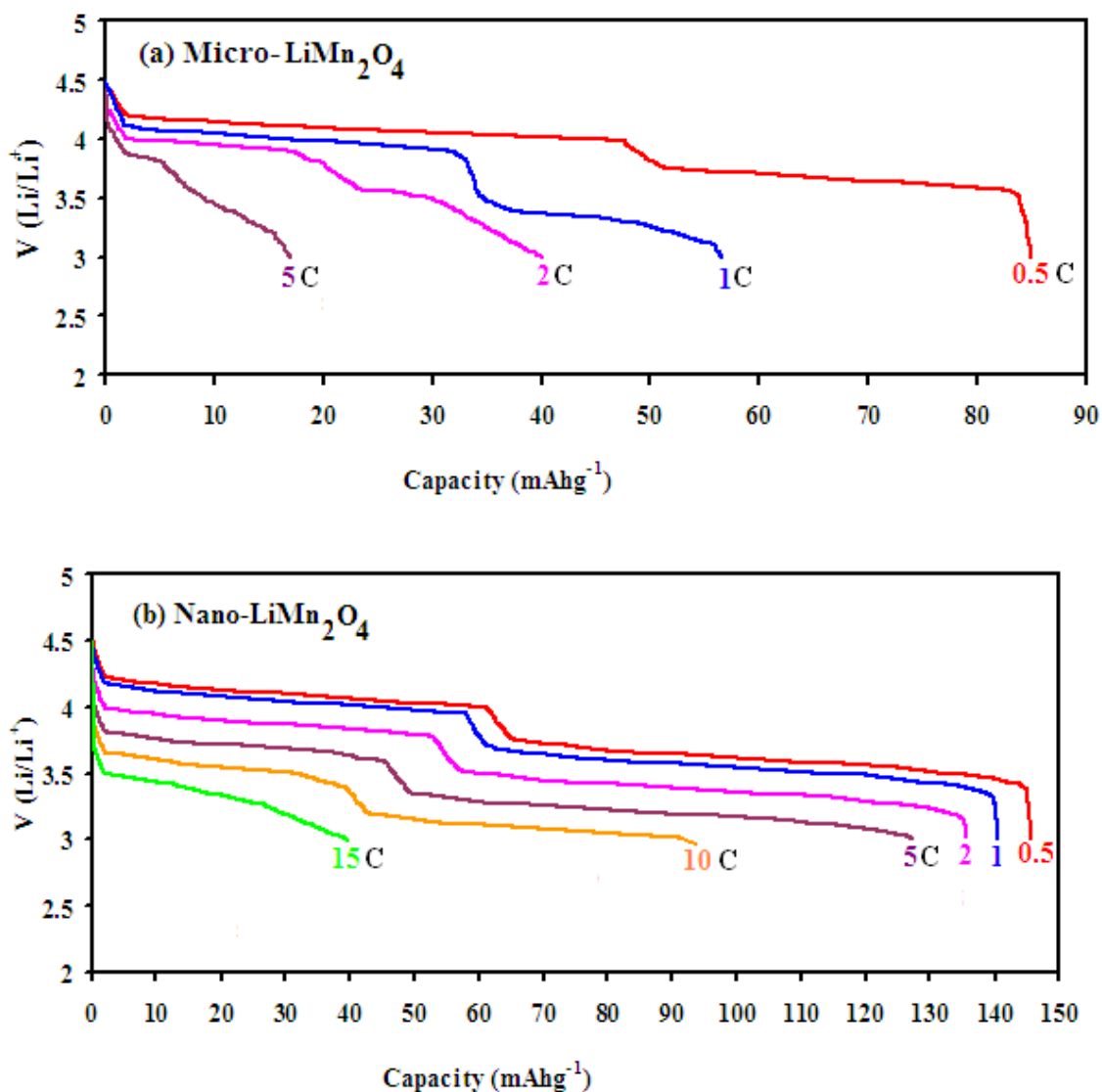


**Figure 6.** Discharge curves of  $\text{LiMn}_2\text{O}_4$  tested at various C rates between 3.0 and 4.5 V. (a) micro-particles and (b) nano-particles.

The cells were charged at a constant rate of 1 C and discharged at different C. Fig. 6 shows the effect of discharge current densities on the capacities of the two types of electrodes. The discharge capacity of both electrodes decreases with increasing discharge current density as expected. However, the decreasing rate for each electrode is different. As shown in Fig. 6(a), the micro-particles delivered

56 mAhg<sup>-1</sup> at a rate of 1 C, and the specific discharge capacity significantly decreased with increasing C rate. At the rate of 2 and 5 C, the discharge capacity decreased to 40 and 17 mAhg<sup>-1</sup>, respectively. In 5 C rate of discharge, the cathode materials have no significant performance. For the nano-particles discharged at 1 C, 94% of the theoretical capacity was delivered (140 mAhg<sup>-1</sup>) as shown in Fig. 6(b). With an increase in the C rates, the discharge capacity slowly decreased. The nano-particles exhibited 135, 127, 98 and 40 mAhg<sup>-1</sup> specific capacities at 2, 5, 10 and 15 C rate of discharge, respectively. Even at high discharge rates (10 and 15 C), the cathode which was made from nano-particles has an acceptable specific discharge capacity. Moreover, the nano-particles had increased surface area and enhanced reactivity due to their nano-scaled sizes. The diffusion length and resistance for lithium ions would be reduced, leading to an improvement in the electrochemical behaviors. The rate capability tests indicate that nano-particles have a great potential for high rate applications.

Besides their excellent high current rate charge/discharge performance, nanostructured electrode materials may also deliver good cycle stability [4, 55, 56]. Fig. 7 shows the cycling life tests of the Li/LiMn<sub>2</sub>O<sub>4</sub> cells at a constant charge/discharge rate of 0.5 C for both micro- and nano-particles of LiMn<sub>2</sub>O<sub>4</sub>.

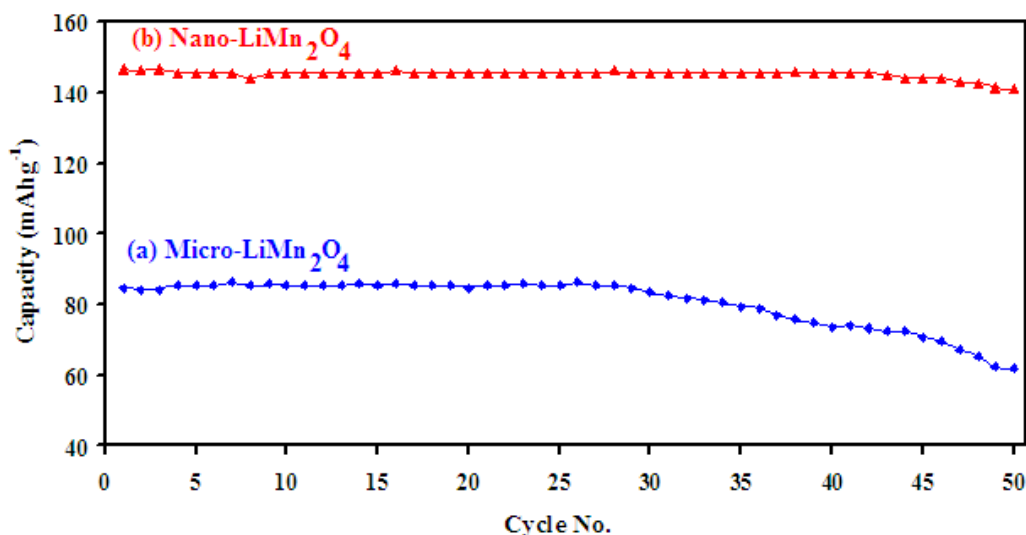


**Figure 7.** Discharge specific capacity curve vs number of cycles for (a) micro-particles and (b) nano-particles at rate of 0.5 C.

As can be seen from this figure, micro-particles (curve a) show lower capacity than nano-particles (curve b) in all cycles. During the subsequent cycles of micro-particles of LiMn<sub>2</sub>O<sub>4</sub>, the capacity will gradually decrease. After 50 cycles, the micro-structured electrode can keep its discharge capacity at 62 mAhg<sup>-1</sup> and 27% of the initial capability is lost (Fig. 7a). As compared with the micro-particles, the nano-particle electrode shows a relatively higher initial discharge capacity and the capacity still remains at 141 mAhg<sup>-1</sup> after 50 cycles and only 3.4% of the capacity is lost (Fig. 7b). It seems that above factors significantly decrease in the case of nano-particles [14]. Some factors which influence the capacity loss during charge/discharge cycling are: (i) electrochemical reactions of

electrolyte solution at high voltage (above 4.0 V); (ii) Jahn-Teller distortion [57, 58]; (iii) dissolution of manganese into the electrolyte according to the disproportionation reaction:  $2\text{Mn}^{3+} \rightarrow \text{Mn}^{4+} + \text{Mn}^{2+}$  [59]. Also a decrease in capacity fade over subsequent cycles is explained by the change in surface area. Intercalation is a process influenced by this parameter because the dimensions of the crystal can affect the surface energy of the materials. The surface area to volume ratio is reversely proportional to the dimension of the particles [15]. This explains the increased efficiency of the intercalation process in the nano materials, that is, an improved performance of about 72% (in the first cycle) and reduced capacity fade over the 50 cycles investigated.

#### 4. CONCLUSION

$\text{LiMn}_2\text{O}_4$  spinel with two different sizes (micro and nano) were synthesized and comparatively studied. Nano-particles of  $\text{LiMn}_2\text{O}_4$  were synthesized by a two-step method that combines sonochemical synthesis of  $\text{MnO}_2$  nano-particles and a solid state reaction to convert them to  $\text{LiMn}_2\text{O}_4$  nano-particles. The average sizes of the particle prepared by this method are observed to be about 35 nm.  $\text{MnO}_2$  micro-particles were synthesized in the presence of stirrer then converted to  $\text{LiMn}_2\text{O}_4$  micro-particles. X-ray analysis showed that pure  $\text{LiMn}_2\text{O}_4$  is produced at 700 °C and in the other temperatures some impurities of manganese oxides are present. Micro- and nano-particles of  $\text{LiMn}_2\text{O}_4$  were used as active cathode material for Li battery. CV and EIS tests demonstrated that electrochemical reversibility and  $\text{Li}^+$  diffusion property of the electrode material with nano-particles are dramatically improved, which is related to the strong interaction of nano-particles with Li ion that occurred mostly at the surface as compared to micro-particles. The lithium cells made from the nano-particles exhibited good performance under different regimes of charge/ discharge rate (from 0.5 C to 15 C) upon cycling from 3.0 to 4.5 V. The utility of nano-material for lithium batteries is a result of the high surface area and porosity and nanometric size of its particles.

#### ACKNOWLEDGEMENTS

We gratefully acknowledge the Tarbiat Modares University Research Council and the Iran National Science Foundation (research grant no. 83135) for supporting this work.

#### References

1. H.K. Song, K. T. Lee, M. G. Kim, L.F. Nazar, J. Cho, *Adv. Funct. Mater.* 20 (2010) 3818.
2. A.C. Dillon, *Chem. Rev.* 110 (2010) 6856.
3. P.G. Bruce, B. Scrosati, J.M. Tarascon, *Angew. Chem. Int. Ed.* 47 (2008) 2930.
4. H. Zhou, D. Li, M. Hibino, I. Honma, *Angew. Chem. Int. Ed.* 44 (2005) 797.
5. J.B. Goodenough, Y. Kim, *Chem. Mater.* 22 (2010) 587.
6. M.S. Whittingham, *Chem. Rev.* 104 (2004) 4271.
7. Y. Wang, G. Cao, *Adv. Mater.* 20 (2008) 2251.
8. H.S. Park, S.J. Hwang, J.H. Choy, *J. Phys. Chem. B* 105 (2001) 4860.

9. D. Kovacheva, H. Gadjov, K. Petrov, S. Mandal, M.G. Lazarraga, L. Pascual, J.M. Amarilla, R.M. Rojas, P. Herrero, J.M. Rojo, *J. Mater. Chem.* 12 (2002) 1184.
10. M. Jayalakshmi, M. M. Rao, F. Scholz, *Langmuir* 19 (2003) 8403.
11. Y. S. Lee, Y. K. Sun, K. S. Nahm, *Solid State Ionics* 109 (1998) 285.
12. B.J. Hwang, C.Y. Wang, M.Y. Cheng, R. Santhanam, *J. Phys. Chem. C* 113 (2009) 11373.
13. M. Okubo, E. Hosono, J. Kim, M. Enomoto, N. Kojima, T. Kudo, H. Zhou, I. Honma, *J. Am. Chem. Soc.* 129 (2007) 7444.
14. K. M. Shaju, P. G. Bruce, *Chem. Mater.* 20 (2008) 5557.
15. N. Kamarulzaman, R. Yusoff, N. Kamarudin, N.H. Shaari, N.A. Abdul Aziz, M.A. Bustam, N. Blagojevic, M. Elcombe, M. Blackford, M. Avdeev, A.K. Arof, *J. Power Sources* 188 (2009) 274.
16. D. K. Kim, P. Muralidharan, H. W. Lee, R. Ruffo, Y. Yang, C. K. Chan, H. Peng, R. A. Huggins, Y. Cu, *Nano Lett.* 8 (2008) 3948.
17. Y.K. Sun, I.H. Oh, K.Y. Kim, *Ind. Eng. Chem. Res.* 36 (1997) 4839.
18. E.I. Santiago, S.T. A. Filho, P.R. Bueno, L.O.S. Bulhoes, *J. Power Sources* 97-98 (2001) 447.
19. C. P. Fonseca, E. M.J.A. Pallone, S. Neves, *Solid State Sciences* 6 (2004) 1353.
20. H.K. Park, G. Kim, *Solid State Ionics* 181 (2010) 311.
21. S.T. Myung, S. Komaba, N. Kumagai, H. Yashiro, H.T. Chung, T.H. Cho, *Electrochim. Acta* 47 (2002) 2543.
22. T. Doia, T. Yahiro, S. Okada, J. Yamaki, *Electrochim. Acta* 53 (2008) 8064.
23. H.J. Choi, K.M. Lee, G.H. Kim, *J. Am. Ceram. Soc.* 84 (2001) 242.
24. N.V. Kosova, N.F. Uvarov, E.T. Devyatkina, E.G. Avvakumov, *Solid State Ionics* 135 (2000) 107.
25. J. Zhang, J. Du, B. Han, Z. Liu, T. Jiang, Z. Zhang, *Angew. Chem.* 118 (2006) 1134.
26. S. F. Wang, F. Gu, M. K. Lu, *Langmuir* 22 (2006) 398.
27. K. S. Suslick, M. Fang, T. Hyeon, *J. Am. Chem. Soc.* 118 (1996) 11960.
28. V. G. Pol, O. Palchik, A. Gedanken, I. Felner *J. Phys. Chem. B* 106 (2002) 9737.
29. D. N. Srivastava, S. Chappel, O. Palchik, A. Zaban, A. Gedanken, *Langmuir* 18 (2002) 4160.
30. B. Gates, B. Mayers, A. Grossman, Y. Xia, *Adv. Mater.* 14 (2002) 1749.
31. J. Geng, J. J. Zhu, D.J. Lu, H. Y. Chen, *Inorg. Chem.* 45 (2006) 8403.
32. T.J. Mason, J.P. Lorimer, *Sonochemistry: Theory, Applications and Uses of Ultrasound in Chemistry*, John Wiley and Sons, New York, 1988.
33. K. S. Suslick, S. B. Choe, A. A. Cichowlas, M. W. Grinstaff, *Nature* 353 (1991) 414.
34. A. Gedanken, *Ultrason. Sonochem.* 11 (2004) 47.
35. K.S. Suslick, G.J. Price, *Ann. Rev. Mater. Sci.* 29 (1999) 295.
36. D. Kovacheva, B. Markovsky, G. Salitra, Y. Talyosef, M. Gorova, E. Levi, M. Riboch, H. Kim, D. Aurbach, *Electrochim. Acta* 50 (2005) 5553
37. X. Fang, Y. Lu, N. Ding, X.Y. Feng, C. Liu, C.H. Chen, *Electrochim. Acta* 55 (2010) 832.
38. M.A. Kiani, M.F. Mousavi, S. Ghasemi, *J. Power Sources* 195 (2010) 5794.
39. M. S. Rahmanifar, M. F. Mousavi, M. Shamsipur, *J. Power Sources* 110 (2002) 229.
40. H. Karami, M. F. Mousavi, M. Shamsipur, *J. Power Sources* 117 (2003) 255.
41. H. Karami, M. F. Mousavi, M. Shamsipur, *J. Power Sources* 124 (2003) 303.
42. M. S. Rahmanifar, M. F. Mousavi, M. Shamsipur, M. Ghaemi, *J. Power Sources* 132 (2004) 296.
43. M.S. Rahmanifar, M.F. Mousavi, M. Shamsipur, H. Heli, *Synthetic Met.* 155 (2005) 480.
44. H. Karami, M. F. Mousavi, M. Shamsipur, S. Riahi, *J. Power Sources* 154 (2006) 298.
45. Kh. Ghanbari, M.F. Mousavi, M. Shamsipur, *Electrochim. Acta* 52 (2006) 1514.
46. Kh. Ghanbari, M.F. Mousavi, M. Shamsipur, H. Karami, *J. Power Sources* 170 (2007) 513.
47. S. Ghasemi, M. F. Mousavi, H. Karami, M. Shamsipur, S.H. Kazemi, *Electrochim. Acta* 52 (2006) 1596.
48. H. Karami, M. Shamsipur, S. Ghasemi, M.F. Mousavi, *J. Power Sources* 164 (2007) 896.
49. H.R. Ghenaatian, M.F. Mousavi, S.H. Kazemi, M. Shamsipur, *Synthetic Met.* 159 (2009) 1717.
50. S. Ghasemi, M.F. Mousavi, M. Shamsipur, H. Karami, *Ultrason. Sonochem.* 15 (2007) 448.

51. Y. Iriyama, M. Inaba, T. Abe, Z. Ogumi, *J. Power Sources* 94 (2001) 175.
52. M. Mohamedi, D. Takahashi, T. Uchiyama, T. Itoh, M. Nishizawa, I. Uchida, *J. Power Sources* 93 (2001) 93.
53. Y. Ding, P. Zhang, D. Gaoc, *J. Alloy. Compd.* 456 (2008) 344
54. Y. S. Hu, L. Kienle, Y.G. Guo, J. Maier, *Adv. Mater.* 18 (2006) 1421.
55. P. Liu, S. Lee, C. Tracy, Y. Yan, J. Turner, *Adv. Mater.* 14 (2002) 27.
56. I. Yamada, T. Abe, Y. Iriyama, Z. Ogumi, *Electrochem. Commun.* 5 (2003) 502.
57. M. Wohlfahrt-Mehrens, C. Vogler, J. Garche, *J. Power Sources* 127 (2004) 58.
58. F.T. Quinlan, K. Sano, T. Willey, R. Vidu, K. Tasaki, P. Stroeve, *Chem. Mater.* 13 (2001) 4207.
59. S.T. Myung, S. Komaba, N. Hirotsuki, N. Kumagai, *Electrochem. Commun.* 4 (2002) 397.